Cavitation Erosion of Some Alloys Manufactured on Steel and Iron Surfaces by Laser Beam

Bolesław G. Gireń and Marek Szkodo

(Submitted 18 June 2002; in revised form 25 June 2003)

Cavitation erosion resistance of structural carbon steel, corrosion resistant chromium steel and technical iron superficially processed by CO_2 laser beam were investigated. Various metallic powders had been alloyed on the surfaces of the samples and then subjected to cavitation at the rotating disc facility. Tests were carried out in the incubation period of the erosion. It was found that material of reduced ability to work hardening could not achieve optional resistance to cavitation, regardless of its hardness. Moreover, strong dependence of the increase in erosion resistance of the alloyed materials on the substrate was also observed. The best performance under the erosion conditions displayed the samples alloyed with AlNi and SiC or with Nb powders. In each case mentioned, high increase in surface hardness was achieved due to cavitation loading.

Keywords cavitation erosion, laser processing

1. Introduction

Cavitation wear of metallic surfaces is a major concern in hydraulic machinery. Controlling cavitation phenomena in field conditions by appropriate machine design and submergence setting is not always applicable. In this case, the protection of solid body against cavitation attack may consist of manufacturing a surface layer of high erosion resistance. Results of numerous works proved that alloying, cladding, melting, or rapid heating of ferrous alloys by laser beam was an effective method leading to an increase in their cavitation resistance.[1-8] However, the problem of protecting hydraulic machine surfaces still remains in many cases unresolved, because the erosion of different iron base alloys is very differentiated[9] and the material resistance to cavitation action depends, among other factors, on intensity of loading and type of impingement.

In the case of low intensity cavitation, as it usually happens in machine operating conditions, the performance of materials in the initial period of erosion is paramount. At that time, the shear components of applied stresses of the impulses are not significant and the energy backscatter in a fluid medium is high. Prolongation of the incubation time (defined as time of almost imperceptible loss of the material mass; e.g., the time marked out by the intersection of the abscissa and the line of extension of linear ascending part of the volume loss curve, or the tangent to cumulative volume loss curve at the inflection point) can be achieved by modification or placing of thin coatings on the metallic surface.

Application of laser techniques to improve the materials erosion resistance should be most effective when the developed microstructures undergo transformations under the cavitation loading,[10] or, on the other hand, are strengthened due to dissolution of the precipitation or second-phase particles. Some amount of fcc crystal structure within the surface layers of tested alloys could also contribute to an increase in cavitation resistance,[11] especially if cavitation wear is regarded as the fatigue process.[12,13]

Laser beam heating and subsequent rapid cooling lead as a rule to grains refining and, due to diffusion retarding, create the state of residual stresses within the processed material. Formation of the hard martensitic structure within the surface layer of steels due to laser processing is the main cause of significant increase in their erosion resistance in the incubation period of cavitation. Refining of the grains and a decrease in microcrack lengths causes the material to erode in smaller pieces and at a lower rate. However, it could be expected that an increase in hardness or tensile strength of steels achieved as a result of laser processing may not decrease the rate of cavitation erosion in the late stage of destruction, due to an inevitable increase in brittleness[14] or lowering of strain hardening capability.[15]

The influence of residual stresses—petrified within the surface layer—on the material performance under cavitation loading depends on the nature of the stresses.[16,17] Residual compression increases the allowed loading and transfers the position of the maximum stress to a substrate location, whereas residual tension weakens the surface.[18] On the other hand, the nature of the residual stresses depends on the material subjected to the processing.[19] Values of residual stresses up to 500 MPa for vertical components and 300 MPa for horizontal components remaining after laser melting of steels 2Cr13 or 45 were detected in Ref. 20 and 21.

In recent years some remarkable attempts have been made to improve the wear properties of steels by enriching their surface layers with various kinds of elements.[8,22,23] However, several technological problems still need to be solved, and understanding of the phenomena needs to increase; therefore, further investigations are needed. Among others, the relationships of the erosion resistance of materials subjected to laser alloying or cladding with properties of the surface layer, type

Bolesław G. Gireń, Institute of Fluid-Flow Machinery Polish Academy of Science 80-952 Gdańsk Fiszera 14, Poland; and **Marek Szkodo,** Technical University of Gdańsk, Faculty of Mechanical Engineering 80-952 Gdańsk Narutowicza 11, Poland. Contact e-mail: giren@imp.gda.pl.

Table 1 Characterization of the Produced Layers

Substrate and Samples Designation	Composition, wt.%, and Thickness of Powder Layers Attached	Actual—Post-Processing—Average Chemical Composition of the Produced Surface Layers[(a)] and Content of Crystalline Phases: Phases of High Probability of Occurrence	Average Thickness of Alloyed Layer, mm
45/1	100.0Nb 0.35 mm	94.88Fe/0.42C/4.7Nb martensite, Nb_6C_5, $Fe_{0,55}Nb_{0,67}$	0.033
45/2	73.0AlNi*/27.0SiC 0.38 mm	74.47Fe/5.17Ni/8.22Al/3.57Si/7.86C/0.71Mn Al and Ni rich phases	0.056
45/3	78.6FeCr*/21.4SiC 0.31 mm	Upper part of the layer 49.58Fe/39.92Cr/5.21Si/6.29C Cr rich ferrite, Cr_5Si_3, FeCr, SiC, Lower part of the layer 77.90Fe/12.06Cr/4.04Si/6.00C martensite, Cr_5Si_3	0.051
45/4	100.0SiC 0.28 mm	86.52Fe/5.37Si/7.69C/0.42Mn martensite, Fe_2C, SiC	0.060
45/5	99.9AlNi*/0.1SiC 0.30 mm	80.15Fe/9.32Ni/10.11Al/0.22C/0.2 Mn heterogeneous microstructure of Al and Ni rich phase, martensite, and $Al_{13}Fe_4$	0.072
2Cr13/1	99.9AlNi*/0.1SiC 0.28 mm	86.55Fe/5.47Ni/6.46Al/0.2C/0.4Cu/0.92Mn Al and Ni rich phase, martensite, FeNi, and eutectics***	0.14
2Cr13/2	72.0AlNi*/27.0SiC 0.33 mm	59.9Fe/10.44Cr/10.39Ni/10.84Al/5.51Si/2.92C austenite and eutectics $Al_{0,9}Ni_{1,1}$, FeNi, SiC	0.049
2Cr13/3	100.0SiC 0.30 mm	79.97Fe/8.23Cr/6.82Si/4.58C/0.40Mn martensite, Fe_2C, SiC	0.17
2Cr13/4	46.7FeCr*/45.29AlNi*/4.0B** 0.35 mm	74.9Fe/22.37Cr/1.55Ni/1.18A/0.10C martensite, FeCr, Fe_2B	0.08
Ar/3	85.81Mn/0.48C/0.96Cr/2.87Ti/4.8Si/4.8Mo/0.28B 0.45 mm	Upper part of the layer 87.7Fe/0.57Cr/1.54Si/0.07C/9.44Mn/0.43Ti/0.25Mo alloy martensite, eutectics***, Fe_2Si Lower part of the layer 92.54Fe/0.40Cr/0.70Si/0.2C/5.80Mn/0.26Ti/0.1Mo martensite	0.116
Ar/4	3.45Mn/6.9C/20.69Nb/3.45Ti/6.90Si/10.34Co/42.27AlNi* 0.39 mm	Matrix 68.29Fe/7.10Ni/8.03Al/2.14Si/0.48C/9.96Nb/0.92Mn/0.35Ti/2.73Co austenite, $Al_{0,9}Ni_{1,1}$ Extrusions 26.46Fe/1.67Si/8.1C/55.44Nb/1.29Mn/5.28Ti/1.75Co	0.137

* Chemical composition of the compound given in Table 2
** The content of boron within the alloyed layer could not be defined
*** Eutectics of undefined phases
(a) Heterogeneity of the produced layers resulted in differentiated content of dissolved elements.

Table 2 Quality Specification of the Powders Used

									Compound		
Powder	**B**	**Co**	**Cr**	**Si**	**Mo**	**Mn**	**Nb**	**Ti**	**FeCr**	**SiC**	**AlNi**
Particle size	<10 μm	<149 μm	<400 μm	<300 μm	<63 μm	<177 μm	<44 μm	<250 μm	<200 μm	<150 μm	<250 μm
Purity	96% B	99.9+% Co	98% Cr	98% Si	99% Mo	99.9% Mn	99.8% Nb	98% Ti	28.3% Fe-63% Cr-7.7% C-1% Si	99% SiC	57.47% Al 41.9% Ni-0.4% Fe-0.2% Si-0.03% Cu

of substrate, and cracking susceptibility of the bonding zone should be examined. The last problem is of great importance in coatings technology.[24]

In this report, the cavitation erosion performance of structural carbon steel (45), corrosion resistant chromium steel (2Cr13), and technical iron (denoted as TI) with some laser-made surface modifications was investigated. The samples melted and alloyed by CO_2 laser beam were subsequently subjected to cavitation loading at the rotating disc facility. The tests were performed in the incubation period of the erosion. The damage of the processed and unprocessed surfaces at any moment of cavitation erosion process was de-

fined (among others) by the areas under the curves of size distributions of indentations. To find out a correlation between the increase in cavitation resistance and the work-hardening capability of the materials, the measurements of surface hardness and in-depth distributions of microhardness of the samples were also done, both before and after the cavitation loading. The investigations were confined to the incubation time of erosion because the role of protective coatings (or modified surface layers) is essential in this period of cavitation.

2. Experimental Procedures

2.1 Objects of Investigations and Processing Procedures

The samples for investigations were made of 0.45% carbon steel (45) of the grades: Fe-0.45C-0.65Mn-0.25Si-0.30Cr-0.30Ni-0.30Cu-0.04P-0.04S. The samples were thermally processed to achieve structural homogeneity. The other samples were 13% chromium steel (2Cr13) of the grades: Fe-0.2C-13Cr-0.6Mn-0.5Si-0.2Ni in soft annealing state, and technical iron (TI) of the grades: Fe-0.01C-0.02Mn-0.03Si-0.03S-0.01P. The appropriate additive (AlNi, Nb, Cr, B, SiC, Mn, Ti, Co, Mo, FeCr) powders were attached to the workpiece surfaces with natrium water glass. Their average thickness is presented in Table 1. The thickness of the samples equaled 0.6 cm and their surfaces were sandblasted. The quality specification of the powders used is presented in Table 2. The powders were selected for the following reasons:

Nb was expected to cause the dispersive hardening and was assumed to form stable carbides contributing to the increase in the material strength. Inserting silicon carbide into the surface layers of the samples was done for its high hardness and unfusibility. The presence of free Si ($\leq$0.16%) in a solution may contribute to an increase in cavitation resistance of the material by removing hydrogen. The alloying with aluminum was anticipated to have a positive effect on grains refining and to reduce the brittleness of the material. Increasing the content of chromium in the surface layers of the samples, accomplished by alloying with FeCr compounds, was expected to form a hard corrosion resistant zone, which is of vital importance in the case of machines subjected to wear and exposed to corrosive media. Boron was incorporated to strengthen the alloys, especially the multiphase structure of the samples depicted as Ar/3. The same refers to titanium. Co was placed into the surface layers of the samples Ar/4 to stabilize and strengthen the lattice of austenitic type and to facilitate relaxation of stresses in the material exploited under cavitation loading. One of the reasons for selection of the alloying elements was the need to design surface alloys of different work hardening capabilities.

Continuous work CO_2 lasers were used as power sources: LPT1.2 (Institute of Fluid Flow Machinery, Gdansk, Poland) described in Ref. 25 and TRIUMPH TLF 6000. The main parameters of the devices, as well as the conditions of the processing, are presented in Table 3. The beam power delivered to the sample surface was attenuated by 3% due to multiple reflections along the optical trail.

During the experimental runs the specimens were moved across the laser beam along some parallel paths, in the case LPT1.2, or along a single 1 cm wide path when processed by TLF6000. The velocities of samples subjected to laser processing ranged from 0.5-0.8 cm/s due to different susceptibility to melting of various powders. Argon of purity 99.998%, 2 ppm of O_2, and 8 ppm of the remaining impurities (N_2, CH_3, H_2, H_2O, CO_2) was used as a shielding gas. The main requirement was the gas shield had to protect the focusing optics from the fumes and the molten material from oxidation. Despite increased diffusivity of the alloying elements within the molten pool at elevated temperatures, the gas composition is not considered an important process variable.[26] A thin surface oxide layer that eventually formed after the processing runs was removed by mechanical polishing.

Due to differences in melting temperatures of alloying elements as well as a relatively slow course of the processing (and resultant convective-diffusive separation of the elements accompanied by evaporation), chemical compositions of the manufactured surface layers differed from that of the substrate powder and were at depth non-uniform. Exemplary line spectra of some alloying elements distributions within the surface layer of 45/2 sample are shown in Fig. 1. The averaged chemical composition of the investigated samples, defined in surface points by electron dispersive spectroscopy (EDS), is presented in Table 1. Laser-treated samples were found to be crack free. Before placing the workpieces into the rotating disk, their surfaces were polished to level the roughness remained after the laser processing.

2.2 Cavitation Testing of the Samples

Afterwards, the processed workpieces were subjected to cavitation impingement at the rotating disk rig.[27] The cavita-

Table 3 Experimental Conditions of Metal Surface Processing

Experimental Setup	LPT1.2	TLF6000
Laser beam power, W	1050	6000
Laser beam mode	TEM 1.0 + TEM 0.1	TEM 0.1
Laser beam diameter, cm	0.8	2.5
Laser beam divergency	1.5-1.7 mrad	1.5 mrad
Focusing element	ZnSe lens	Kugler mirror optics for the formation of the laser beam field uniformly on the area 1 × 10 mm
Focal length, cm	8.9	20
Diameter of the beam spot on the surface, cm	0.16	Rectangular 1 × 10
Sample velocity, cm/s	0.6	0.8
The shielding gas	Argon (99.998%)	Argon (99.998%)
Gas velocity, m/s	47	60

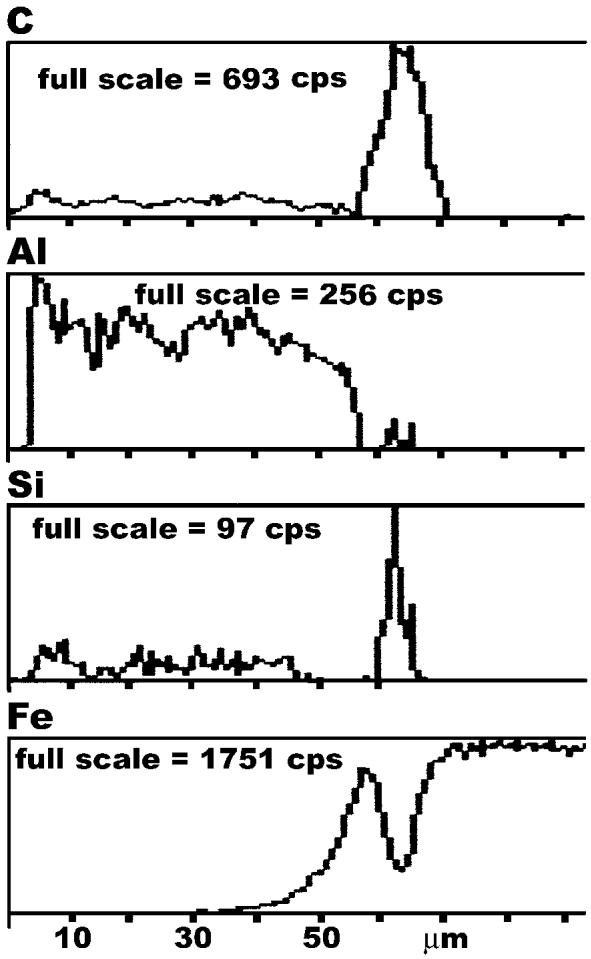

Fig. 1 EDS line spectra of alloying elements within the surface layer of the sample 45/2. On abscissa a distance from the sample surface is marked. Full scale of the vertical axis in each picture refers to the number of impulses depicted above. The scans were conducted on polished cross-section of the sample.

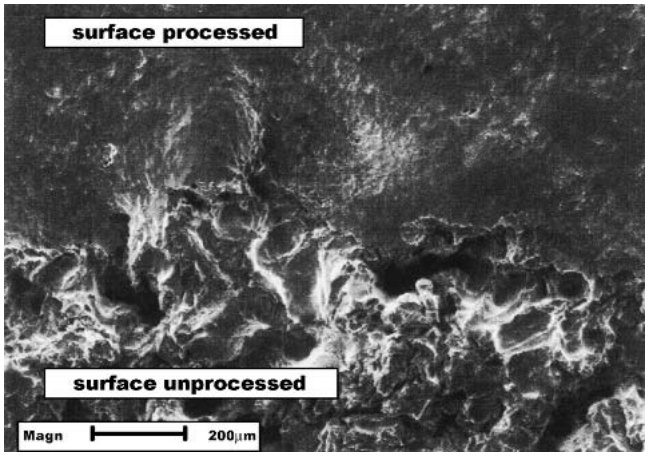

Fig. 2 Surface of the sample Ar/4 after 64 min of cavitation. Upper strip-the area melted and enriched with additives

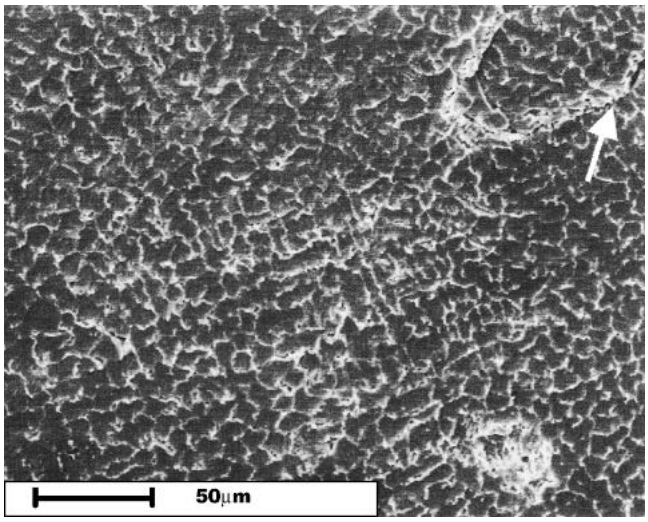

Fig. 3 Surface of the sample Ar/3 after 39 min of cavitation. Structure of the material was revealed due to mechanical etching. Brittle cracking (depicted by arrow) on the surface is visible.

tion was generated by cylinders situated on a circular disk surface of 300 mm in diameter. Test specimens were inlaid in the disk downstream of the cavitator. The rotation speed was 3000 rpm. The resulting mean gauge pressure was 155 kPa. The water temperature of 20 °C was used as an active medium. The tests were performed in 3-6 min runs long following one another, lasting 56 min in total. The duration of each run was less than the time needed to achieve the steady state cavitation intensity.

After each run the indentations of various dimensions exerted by cavitation impact were counted both for processed and reference specimens. The area observed at a given time resulted from the optical magnification and equaled 1.8 × 2.2 mm. However, the craters were detected from the area of two such (detached) rectangles. Indentations of various sizes were counted by MultiScan Base program. The size distributions of the pits were then plotted. To trace the time changes of cavitation resistance of the samples, the quantity $\eta = (Nref-N)/Nref$ was calculated and plotted as a function of time, where N is the area under the size distribution of the pits registered on the alloyed surface, and Nref the area under the size distribution of the pits on the reference (not processed by laser beam) material. The method of quantifying the cavitation damage of materials by counting the pits is admitted in the incubation period of the erosion, such as Ref. 28. When the impingements ceased to be discernible, N and Nref were defined as surface roughness length increment (by profilograph).

An inaccuracy in assessment of η values is included within the experimental points depicted in the plots. The cavitation experiments consisted of the series of runs and the conditions could differ at each series due to a possible change of fluid flow parameters and a limited time of stabilization of cavitation wires. However, it should have had no influence on the value of η for the reference samples were subjected to the same cavitation impingements. The divergence of pits counting on the areas of approximate erosion intensities was a potential source of errors.

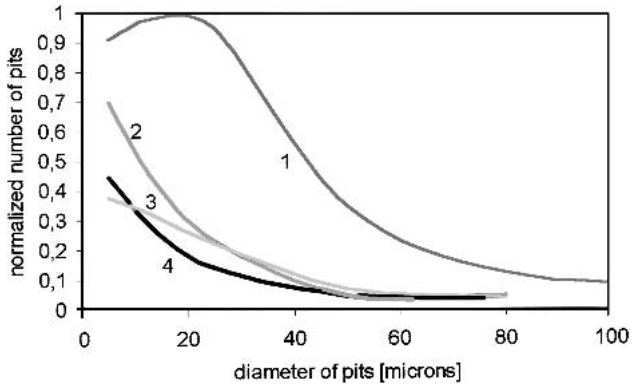

Fig. 4 Size distributions of pits appeared on steel 2Cr13 after 30 min of cavitation: 1, sample not processed; 2, sample 2Cr13/3; 3, sample melted superficially by laser beam; 4, sample 2Cr13/2

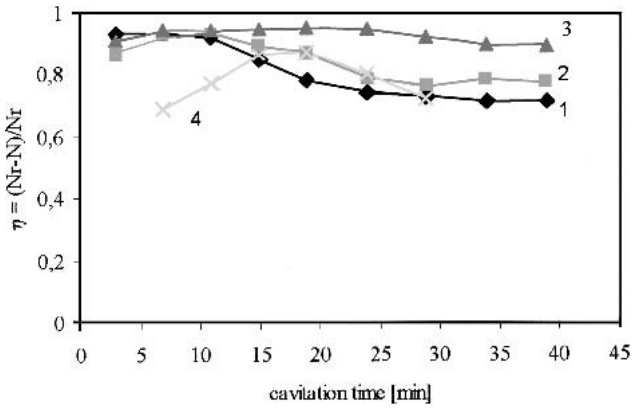

Fig. 5 Time variations of cavitation erosion resistance (defined by index η) of steel 45. 1, sample melted superficially by laser beam; 2, sample 45/1; 3, sample 45/2; 4, sample 45/5

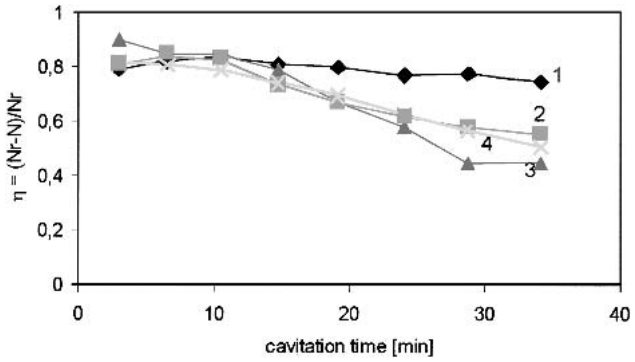

Fig. 6 Time variations of cavitation erosion resistance (defined by index η) of steel 2Cr13. 1, sample 2Cr13/2; 2, sample 2Cr13/1; 3, sample 2Cr13/4; 4, sample melted superficially by laser beam of 1.9 kW

2.3 Material Investigations

A scanning electron microscope Philips 30/ESEM (Philips, Amsterdam-Brno, Holland) was used to visualize both the specimen surface deformations and microstructures in the plane normal to the processing path. Chemical composition

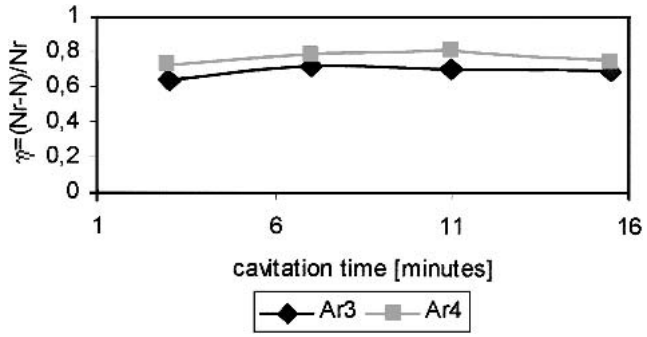

Fig. 7 Time variations of cavitation erosion resistance (defined by index η) of the samples Ar/3 and Ar/4

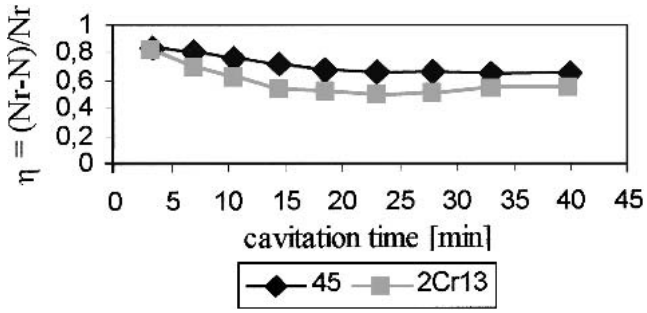

Fig. 8 Time variations of cavitation erosion resistance (defined by index η) of the samples alloyed superficially with SiC: 45, sample 45/4; 2Cr13, sample 2Cr13/3

analysis was carried out by electron dispersive spectroscopy (EDAX). The analysis of the chemical composition at the surface of the tested samples was done at the accelerating voltage of 25 kV. Crystalline phases were detected with the x-ray diffraction method. A Philips PW3040/00 X'Pert MPD was used to carry out the analysis at monochromatic radiation of $\lambda_{CuK\alpha}$ = 15.42 nm.

Hardness was measured by means of a Vickers tester. The microhardness within the processed zone was detected at the load of 2N (HV0.2).

3. Results and Discussion

A typical illustration of the eroded workpiece is presented in Fig. 2. The smooth surface of the laser-melted area can be observed next to the very rough surface of unprocessed part of the sample. At the beginning of the series of test runs the pits were easily discernible. In the late stage of testing, the plastic deformations observed on the surface overlapped, making the pits counting difficult. In some cases the random cracking occurred on a thin and brittle deposited layer (Fig. 3). Pits of different sizes (from 2-50 μm) could be identified. The pits size distributions were found to be different for the transformed and untransformed surfaces. An exemplary set of pit distributions is presented in Fig. 4. In time, damages develop predominantly within the indentations and craters, and the method of assessment of η may fail in the late stage of the erosion.

The series of cavitation erosion curves [i.e., time variations of η = (Nref-N)/Nref quantity] for steels 45, 2Cr13, and TI

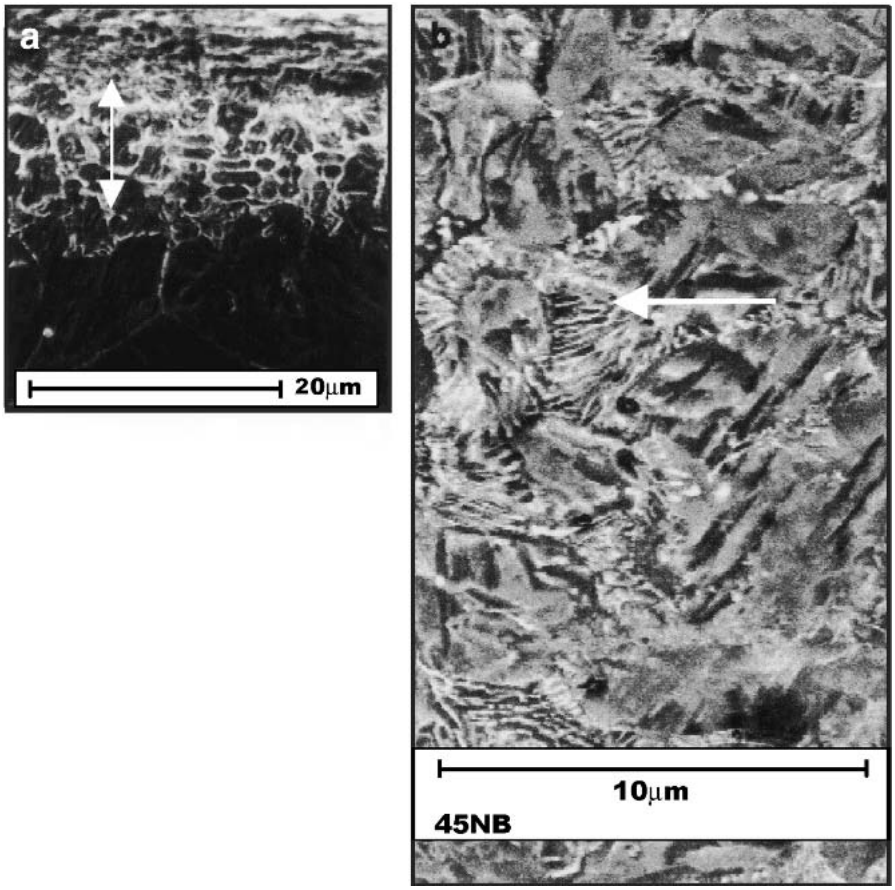

Fig. 9 **(a)** Transit zone (depicted by arrow) between alloyed surface layer and martensitic heat affected zone in sample 45/1; **(b)** refined slab and needle microstructure of the near surface part of the sample 45/1, formed by martensite and phases containing niobium (depicted by arrow).

iron with chemical compositions of the surface layers changed by laser beam are presented in Fig. 5, 6, 7, and 8. Steel 45 in the normalized state and steel 2Cr13 after softening stand for reference materials for the samples 45/1-5 and 2Cr13/1-4. Acid resistant low carbon chromium-nickel steel 0.1C/18Cr/9Ni/0.1Ti subjected to quenching at 1050 °C served as a reference material for the remaining samples (samples with substrates made of TI iron). In all cases, cavitation resistance of the processed samples considerably exceeded the cavitation resistance of reference material even after 40 min of intensive cavitation loading.

An increase in cavitation resistance of steel 45 due to laser alloying was found to exceed an increase in cavitation resistance of steel 2Cr13 (for the same composition of the powders used for alloying; compare the curves in Fig. 8, or curve 3 in Fig. 5 and curve 1 in Fig. 6). A significant influence of the core material type on the cavitation performance of the superficially alloyed samples was observed especially at the beginning of the erosion process, which presumably can be attributed to different intensity of scattering of elastic energy by different substrates. Other supposed reasons are related to the effects of the processing thermal cycle: (1) generation of different residual stress fields at a joint zone; (2) formation of heat affected zones of different strength; (3) formation of bonding zones of different properties due to different phase composition (Fig. 9a, 10a), e.g., a thick martensitic heat affected zone in steel 45 was found to make crack development difficult (Fig. 10) when the coating was brittle.

An increase in η during the first minutes of cavitation loading-observed for the samples 45/1 and 45/5 (curves 2 and 4 in Fig. 5) or 2Cr13/1 and 2Cr13/2 (curves 2 and 3 in Fig. 6)-was due to the work hardening effect. Other samples exhibited rather brittle behavior and did not show considerable change in hardness.

The dependence of η on the material hardening, caused by cavitation impingements, is presented in Fig. 11. In this case η was the average values determined from 10-25 min of cavitation. The considered materials were divided into three groups of alloys selected for their hardness. The first one included alloys of the average surface microhardness (HV0.2) ranging between 470-520 HV. The surface microhardness of materials numbered to the second group was in the 640-700 HV range, and the microhardness specific for the last group was between 790-850 HV. In each case the greater values of η were found when the increase in surface microhardness due to cavitation action was greater. It seems that material of reduced work hardening ability could not achieve optional resistance to cavitation, regardless of its hardness.

In most cases the simultaneous increase in hardness and strain hardening ability is hardly achievable. Grain refining due to laser surface processing makes the work hardening of the

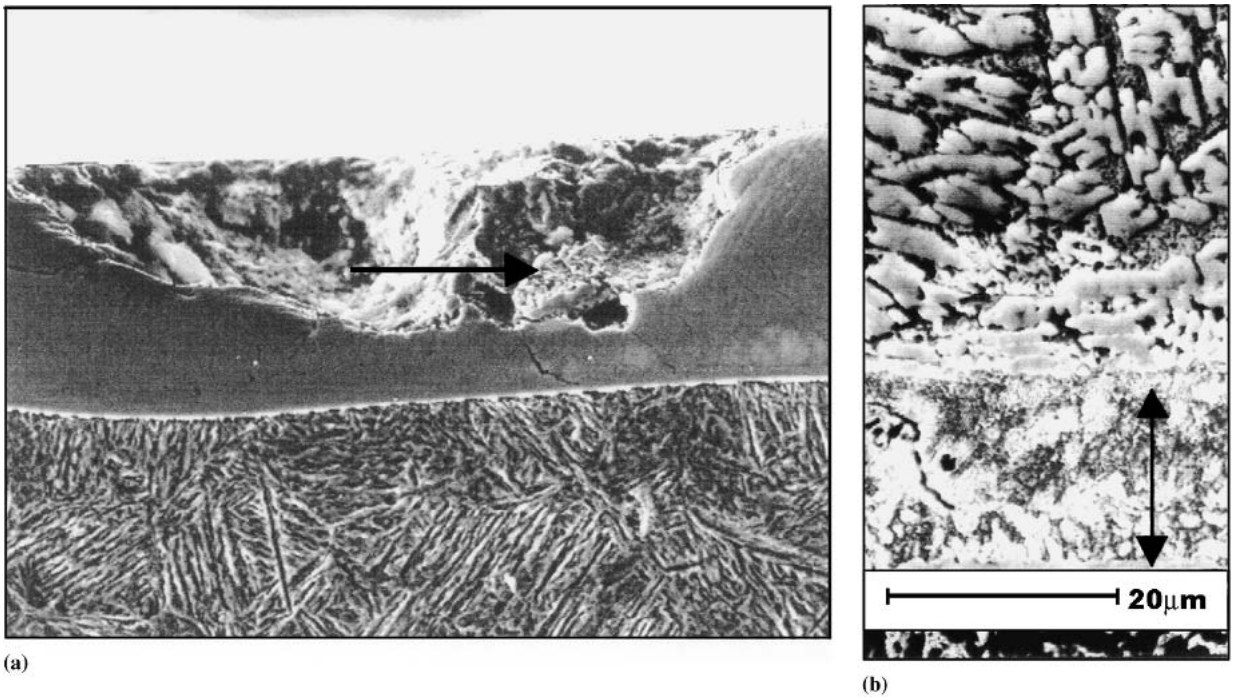

Fig. 10 **(a)** Coating made of compounds FeCr and SiC deposited on the sample 45/3 and supported by a martensite of heat-affected zone. Indentation and crack (depicted by arrows) caused by cavitation impingements are visible; **(b)** microstructure of the same coating revealed by etching. Stresses are concentrated within the down part of the layer (depicted by arrows).

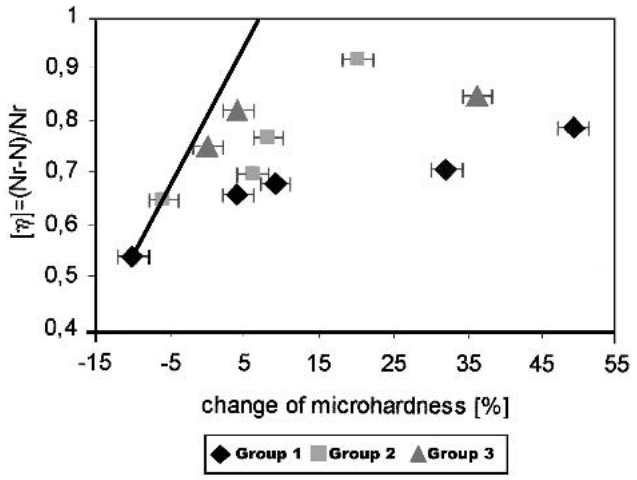

Fig. 11 A set of average values of indicator η for various samples. Each point refers to any particular sample. A variable represented in abscissa is the change of surface microhardness due to cavitation loading. Three groups of materials were selected with respect to the surface hardness. The points in diagram from left to right represent the following alloys: group 1 (470-520 HV0.2) 1-2Cr13/3, 2-Ar/4, 3-45/4, 4-2Cr13/1, 5-2Cr13/2; group 2 (580-700 HV0.2) 1-2Cr13/4, 2-martensite produced due to laser melting of steel 2Cr13, 3-Ar/3, 4-45/2; group 3 (790-850 HV0.2) 1-45/3, 2-martensite produced due to laser melting of steel 45, 3-45/1.

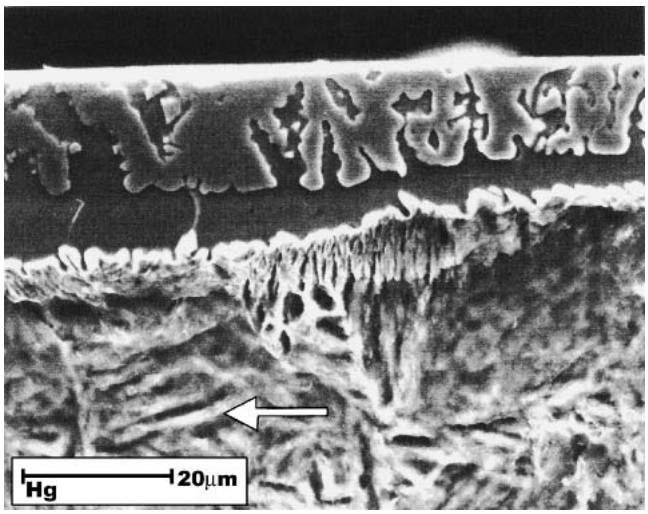

Fig. 12 Surface layer of the sample 45/2. It consists of thin coatings supported on martensite of heat-affected zone. An image of martensite lathings (depicted by arrow) is dull due to the presence of residual stresses.

material more effective.[29] On the other hand, precipitation and other hard phases contribute to the increase in metal hardness, but also deteriorate its ability to work hardening by increasing the stacking fault energy, which may be significant to fatigue erosion.[30] Furthermore, the refining of carbide or boride particles due to high cooling rate (as in our case) leads to the reduction in elongation and strain energy and deteriorates cavitation erosion resistance.[31]

An increase in the erosion resistance of samples alloyed with AlNi+SiC powders (samples 45-2 and 2Cr13-2; Fig. 12, 13) proved to be very durable and stable.

A beneficial effect of laser alloying of TI iron (samples Ar/3

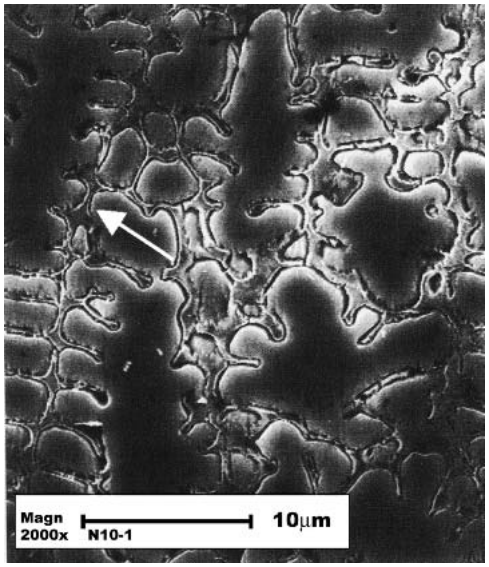

Fig. 13 Microstructure of surface layer of the sample 2Cr13/2. Dendritic configuration of grains with low energy rounded boundaries (depicted by arrow) is specific.

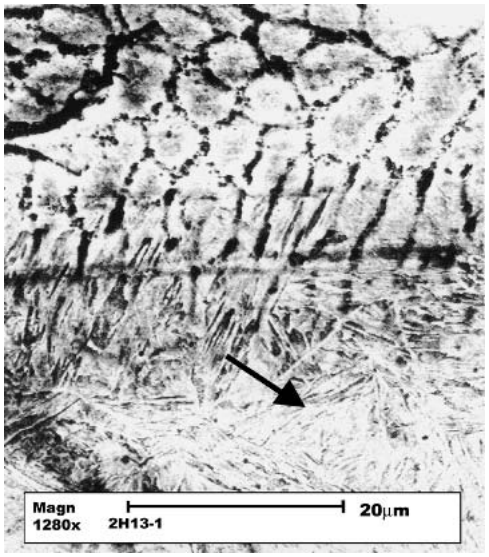

Fig. 14 Microstructure of surface layer of the sample Ar/3. Martensite was formed within the down part of alloyed layer (depicted by arrow).

and Ar/4) was proved by the curves in Fig. 7. The metallographic structures of the samples were shown in Fig. 14 and 15. Results indicate that very high cavitation resistance, much higher than the resistance of reference steel, could be obtained for the samples with the surface layer deposited on much less resistant substrate.

4. Conclusions

1) Both the hardness of the material and its strain hardening ability play a significant role in its cavitation resistance during the incubation period of erosion. Material of reduced ability to work hardening could not achieve optional resistance to cavitation, regardless of its hardness. The strong dependence of erosion performance of laser-produced alloys on their ability to work hardening occurs in not very hard or ductile materials. However, it is probable that alloys of similar surface microhardness exhibit a monotonical relationship between erosion resistance and their ability to work hardening, no matter how brittle or ductile the materials are.
2) The type of the substrate material plays a significant role in cavitation resistance of superficially processed steels.
3) The microalloying of steel with a few percent (weight) of aluminum and nickel and a slight amount of SiC contribute considerably to an increase in both strain hardening efficiency and cavitation resistance of the materials. The erosion performance of the superficially processed samples also seems to be improved due to the presence of manga-

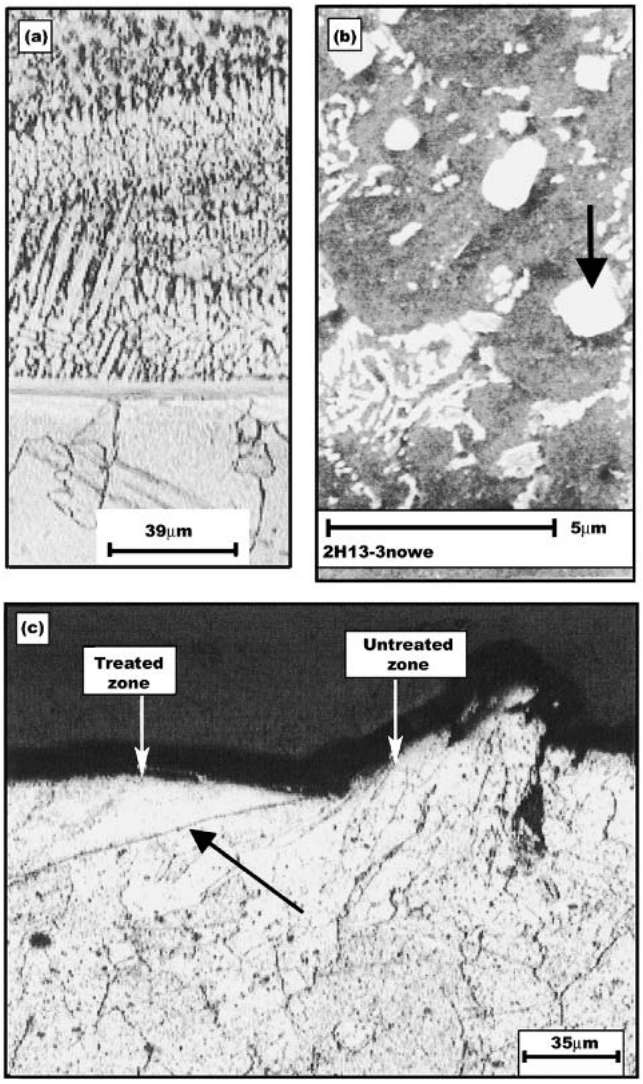

Fig. 15 **(a)** Microstructure of surface layer of the sample Ar/4 deposited on technical (TI) iron; **(b)** precipitation of niobium rich phases (depicted by arrow); **(c)** cavitation damage at the boundary of alloyed zone (depicted by arrow) after 30 min of the erosion

nese (of amount appropriate for austenite formation) or niobium (up to few wt.%). The hard phases in excessive amount confine the possibility of the material hardening under the cavitation loading and can also deteriorate the erosion resistance due to local accumulation of the generated stresses.

Acknowledgment

This work was financed by the Polish Committee for Scientific Research within Project 7 T08C 012 19.

References

1. C.M. Preece and C.W. Draper: "The Effect of Laser Quenching the Surfaces of Steels on Their Cavitation Erosion Resistance," *Wear,* 1981, *67*(3), pp. 321-28.
2. W.J. Tomlinson, J.H. Megaw, A.S. Bransden, and M. Girardi: "The Effect of Laser Surface Melting on the Cavitation Wear of Grey Cast Iron," *Wear,* 1987, *116,* p. 249.
3. W.J. Tomlinson, R.T. Moule, J.H. Megaw, and A.S. Bransden: "Cavitation Wear of Untreated and Laser-Processed Hardfaced Coatings," *Wear,* 1987, *117,* p. 103.
4. S.P. Gadag and M.N. Srinivasan: "Cavitation Erosion of Laser Melted Ductile Iron," *J. Mater. Process. Technol.,* 1995, *51*(1-4), pp. 150-63.
5. D. Dube, M. Fiset, R. Laliberte, and R. Simoneau: "Cavitation Resistance Improvement of IRECA Steel via Laser Processing," *Mater. Lett.,* 1996, *28,* pp. 93-99.
6. B.G. Gireń: "Cavitation Erosion of Steels Processed With a Laser Beam and Optical Discharge Plasma," *Surf. Eng.,* 1998, *14*, p. 325.
7. B.G. Gireń and M. Szkodo: "On the Increase of Cavitation Resistance of A1 Structure Alloys Processed by Laser Beam," *J. Tech. Phys.,* 1999, *XL,* p. 277.
8. C.T. Kwok, F.T. Cheng, and H.C. Man: "Laser Surface Modification of UNS S31603 Stainless Steel Using NiCrSiB Alloy for Enhancing Cavitation Erosion Resistance," *Surf. Coat. Technol.,* 1998, *107,* p. 31.
9. H.G. Feller and Y. Kharrazi: "Cavitation Erosion of Metals and Alloys," *Wear,* 1984, *93,* pp. 249-60.
10. R.H. Richman: "Deformation-Induced Martensite and Resistance to Cavitation Erosion," *J. Phys. IV,* 1995, *5*(C8), pp. 1193-98.
11. W.T. Fu, Y.B. Yang, T.F. Jing, Y.Z. Zheng, and M. Yao: "The Resistance to Cavitation Erosion of CrMnN Stainless Steels," *J. Mater. Eng. Perform.,* 1998, *7*, pp. 801-04.
12. R.H. Richman and W.P. McNaughton: "Correlation of Cavitation Erosion Behavior With Mechanical Properties of Metals," *Wear,* 1990, *140,* pp. 63-82.
13. R.H. Richman and W.P. McNaughton: "A Metallurgical Approach to Improved Cavitation-Erosion Resistance," *J. Mater. Eng. Perform.,* 1997, *6,* p. 633.
14. N.B. Dahotre, A. Hunter, and K. Mukherjee: "Laser Surface Melting of W2 Tool: Effects of Prior Heat Treatment," *J. Mater. Sci.,* 1987, *22,* pp. 403-06.
15. D.R. Rao, B. Ventakaraman, M.K. Asundi, and G. Sundararajan: "The Effect of Laser Surface Melting on the Erosion Behaviour of a Low Alloy Steel," *Surf. Coat. Technol.,* 1993, *58,* p. 85.
16. Y. Terauchi, H. Matuura, and M. Kitamura: "Correlation of Cavitation Damage Tests With Residual Stress Measurements," *Bull. JSME,* 1973, *16,* pp. 1829-40.
17. H. Krause and M. Mathias: "Investigation of Cavitation Erosion Using X-Ray Residual Stress Analysis," *Wear* 1987, *119,* pp. 343-52.
18. R. Priestner and D.M. Priestner: "Importance of the Substrate in Surface Engineering," *Surf. Eng.,* 1991, *7*(1), pp. 53-59.
19. M.R. James, D.S. Gnanamuthu, and R.J. Moores: "Mechanical State of Laser Melted Surface," *Scripta Metall.,* 1984, *18,* p. 357.
20. M. Szkodo and B.G. Gireń: "On the Variations of Residual Stresses in Steels Under the Cavitation Attack," *Mar. Technol. Trans.,* 2001, *12,* pp. 253-64.
21. B.G. Gireń, M. Szkodo, and J. Steller: "The Influence the Residual Stress on Cavitation Resistance of Metals," *Wear,* 1999, *233-235,* pp. 86-92.
22. B.S. Mann: "Boronizing of Cast Martensitic Chromium Nickel Stainless Steel and Its Abrasion and Cavitation-Erosion Behavior," *Wear,* 1997, *208,* pp. 125-31.
23. B.G. Gireń and M. Szkodo: "Cavitation Resistance of 45 and 2Cr13 Steels Enriched Superficially With Laser Deposited Hf, SiC or AlNi+SiC Powders," *SPIE Proc.,* 2000, *4238,* pp. 142-48.
24. W. Song, P. Zhu, and K. Cui: "Effect of Ni Content on Cracking Susceptibility and Microstructure of Laser-Clad Fe-Cr-Ni-B-Si Alloy," *Surf. Coat. Technol.,* 1996, *80,* pp. 279-82.
25. G. Rabczuk, P. Kukiełło, and G. Śliwiński: "Gain and Saturation Intensity Parameters in a Transverse-Flow CO_2 Laser," *Optics Laser Technol.,* 1995, *27,* p. 131.
26. P.J. Oakley: "Practical Aspects of Laser Processing" in *Laser Processing in Manufacturing*, R.C. Crafer and P.J. Oakley, ed., Chapman & Hall, 1993, p. 276.
27. K. Steller, T. Krzysztofowicz, and Z. Reymann: "Effects of Cavitation on Materials in Field and Laboratory Conditions," ASTM, Spec. Tech. Publ., 1975, *567,* p. 152.
28. B. Belahadji, J.P. Franc, and J.M. Michel: "Analysis of the Cavitation Erosion Pits," *Trans. ASME J. Fluid Eng.,* 1991, *113,* p. 700.
29. R.W. Honeycombe: *The Plastic Deformations of Metals,* E. Arnold, ed., 1968, p. 238.
30. D. Kuhlmann-Wilsdorf: *Work Hardening in Tension and Fatigue,* A. Thompson, ed., AIME, 1968, p. 97.
31. M.G. DiVirnieri Cuppari, F. Wischnowski, D.K. Tanaka, and A. Sinatora: "Correlation Between Microstructure and Cavitation Erosion Resistance of High Chromium Cast Steel," *Wear,* 1999, *225-229,* pp. 517-22.